ACS APPLIED ENERGY MATERIALS

www.acsaem.org Article

Potential-Controlled Switchable-Resistance Polymer Layer for Enhanced Safety of Lithium-Ion Batteries with NMC-Type Cathodes

Evgenii V. Beletskii, Alexey I. Volkov, Elena V. Alekseeva, Dmitrii V. Anishchenko, Alexander S. Konev, and Oleg V. Levin*

Cite This: https://doi.org/10.1021/acsaem.3c02145 Read Online

ACCESS | Metrics & More | Article Recommendations | Supporting Information

ABSTRACT: Preventing thermal runaway in lithium-ion batteries is crucial to ensure their safe operation. In this study, we report application of a poly[Ni(CH_3Osalen)] polymer layer at the current collector to protect active materials in high-performance energy storage devices based on NMC532 cathodes. Poly[Ni(CH_3Osalen)] has a conductivity window matching well the operational voltage of NMC materials, and it transitions to a nonconducting state when the potential exceeds safe limits upon overcharge, overdischarge, or short circuit. According to the stress tests performed in coin prototypes and *ex situ* XPS, EDX, and XRD studies, the polymer layer effectively limits current flow under extreme conditions and prevents degradation of internal components of the cell. While securing operational safety of the cell, the polymer layer allows for retention of up to ca. 90% of the capacity value of unprotected samples at an extended operational voltage range of 2.8−5.0 V. According to electrochemical impedance spectroscopy, the protective action of poly[Ni(CH_3Osalen)] stems from the 10-fold increase in the charge transfer resistance at the polymer layer/cathode material interface, which compensates the sharp voltage change.

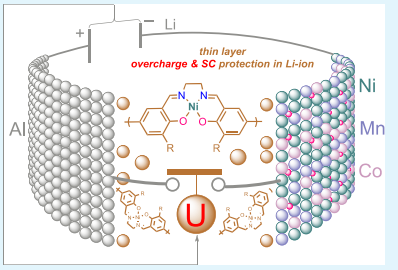

KEYWORDS: *lithium-ion batteries, battery safety, protective layers, NMC532, safety engineering*

INTRODUCTION

Safety and reliability are critical qualities for the commercial use of lithium-ion batteries. Overcharge, short circuit, and thermal or physical abuse damage the battery components[1−5] and can cause ignition or explosion, necessitating careful consideration of every part of the device from a safety perspective.

The existing protection solutions can be grouped into two approaches. The first approach implies external protection through a sophisticated battery management system that combines multiple sensors, actuators, and controllers to monitor the state of the battery and to adjust the operational parameters accordingly.[4,6,7] The second approach is to provide internal protection through chemical modification of the lithium-ion cell. Within this approach, specific electrolyte additives prevent lithium dendrite formation,[8−10] either polymerizable electrolyte additives[11−13] or fusible separators[14−16] trigger the device shutdown at thermal extremes, while voltage-sensitive separators[17,18] and redox shuttle electrolyte additives[19−21] prevent overcharging of the device. Another option is to place a thermoresponsive conductive smart polymer layer between the cathode material and the current collector, which would endow the device with the shutdown control similar to fusible separators or polymerizable additives.[11,16,22−24]

Layered lithium Ni−Mn−Co oxides $Li_{1+x}(Ni_yMn_zCo_{1-y-z})_{1-x}O_2$ (NMC) are promising cathode materials for lithium-ion batteries of high energy density.[25,26] These materials can operate at an average potential of 3.6 V and up to 3.8 V for nickel-rich oxides.[27] The safe range of operation is limited by a 2.8−4.2 V potential window. Above 4.4 V, the decomposition of the cathode material occurs,[28] while a further increase in potential leads to electrolyte degradation.[29] Application of voltage-sensitive separators or redox shuttles in electrolytes could help to keep the NMC-based devices within the safe range of potentials. However, voltage-sensitive separator coatings reported so far[17,18] are known to decompose in contact with metallic lithium, while redox shuttle additives[19−21] narrow the applicable potential window.

In recent reports from our group,[30,31] Beletskii et al. proposed the use of a switchable-resistance layer of polymerized nickel salen complex, poly[Ni(CH_3Osalen)], to protect LFP-based cathodes against overcharging.[30] The approach has garnered interest, with Li et al. using a poly(3-butylthiophene) layer that successfully protected an NCM811-based electrode from overcharging to 4.9 V.[32] Unfortunately, the high onset potential of the resistance change led to unwanted processes in the electrolyte and to irreversible

Received: August 25, 2023
Revised: October 16, 2023
Accepted: October 17, 2023

overoxidation of the polymer with significant loss of conductivity and subsequent device failure. As compared to the work of Li et al., the approach of Beletskii et al. showed protection against short-circuiting as an additional benefit.[31]

Poly[Ni(CH_3Osalen)], which protected $LiFePO_4$ electrodes[30] by switching to a nonconducting state, is activated when the electrode potential exceeds 4.4 V vs Li/Li^+,[33] making it a suitable candidate for protection of NMC-based materials, as the switching of poly[Ni(CH_3Osalen)] films to nonconducting state conveniently coincides with the upper boundary of the NMC working potential window.

This study explores the applicability of poly[Ni(CH_3Osalen)] as a protective option for promising yet demanding NMC-based cathode materials. We analyze the changes occurring in the electrochemical response of electrodes based on NMC532 upon stress tests, including charging at a cell voltage expanded up to 5.0 V, exceeding the normal cycling window by 0.8 V, and external short-circuits. We also provide evidence supporting the benefits of using poly[Ni(CH_3Osalen)] films for battery overcharge protection under extreme conditions (up to 8.0 V).

EXPERIMENTAL SECTION

Anhydrous solvents and electrolytes were purchased from Sigma-Aldrich. Acetonitrile and acetonitrile-based electrolytes were dried over 3 Å molecular sieves. A [Ni(CH_3Osalen)] monomer was synthesized according to a procedure reported before.[34] Lithium nickel manganese cobalt oxide $Li(Ni_{0.50}Mn_{0.30}Co_{0.20})_2O_2$ (typically referred to as NMC532, abbreviated as NMC further in the text for clarity) was provided by local suppliers. Carbon black Super-P was purchased from Alfa Aesar, and PVDF (polyvinylidene fluoride) "Solef 6010" was purchased from Solvay. Aluminum foil (Hefei Kejing Material Technology) was used as an electrode material substrate, and Celgard 2400 (Celgard) was used as a separator.

All cell assembly and open cell measurements were conducted in a glovebox under an argon atmosphere.

Protective Layer Preparation. A poly[Ni(CH_3Osalen)] film was deposited onto a 25 × 18 mm^2 graphitized aluminum foil sheet from a 10 mmol dm^{-3} solution of the monomer in a 1 mol dm^{-3} $LiClO_4$ solution in acetonitrile at a potential of 0.8 V (vs $Ag/AgNO_3$). A graphitized aluminum foil was used as a substrate for electrochemical deposition of the polymer coating to improve the adhesion of the polymer film. The $Ag/AgNO_3$ MF-2062 BASi reference electrode was calibrated as 0.3 V against the Ag/AgCl aqueous reference electrode. The material composed of 80 wt % LTO, 10 wt % carbon black, and 10 wt % PVDF wrapped in a Celgard 2400 separator served as a counter electrode. The thickness of the layer was controlled by the charge passed through the cell and was estimated to be ∼1 μm. The deposited film was rinsed with dry acetonitrile and dried under argon at room temperature for 24 h.

Cathode Material Preparation. Electrode materials were prepared by mixing NMC, carbon black, and PVDF powders in a 90:7:3 weight ratio and dispersing them in *N*-methylpyrrolidone (2.4 mL of solvent per 1 g of dry components) using a Ningbo Hinotek FSH-2A homogenizer (10^4 rpm for 10 min). The slurries were coated onto either aluminum foil or a polymer-coated aluminum foil using a blade applicator. The coatings were then dried in vacuo at 80 °C for 24 h. The obtained coatings were calendered by using a roll press. The mean mass loading was 40 mg cm^{-2}. The samples without the protective coating are referred to as Al/NMC in the text, while the samples with the protective coating are denoted as Al/poly/NMC.

Cell Assembly. Cathode materials were cut into 12 mm disks and assembled in CR2032 cases with 14 mm lithium foil disks and 16 mm Celgard 2400 separators. $LiPF_6$ solution (0.1 mL, 1 mol dm^{-3}) in EC:DEC (1/1 v/v) per cell was used as electrolyte. The cells were assembled by using an MTI MSH-160E crimping machine.

Standard Electrochemical Tests. Galvanostatic charge−discharge (GCD) measurements were performed on a Neware BTS-3000 battery testing system. Cyclic voltammetry (CV), electrochemical impedance spectroscopy (EIS) experiments, and stress tests were performed with a Biologic BCS-805 potentiostat-galvanostat.

GCD data were recorded for a series of five cells for each batch; then, the results were averaged, and the confidence intervals were calculated using Student's *t*-test. GCD was performed in symmetrical mode at current rates from 0.1C to 3C in the 2.8 to 4.2 V potential range (vs Li/Li^+). Cyclic stability of the materials was evaluated at 0.5C.

CV experiments were performed in the 2.8−4.2 V potential range with a scan rate of 0.05 mV s^{-1}.

All EIS spectra were recorded at an open-circuit potential (after discharge to 2.8 V) in the 10 kHz to 10 mHz frequency range with an amplitude of ΔE_{rms} = 10 mV.

Stress Tests. A series of comparative tests were performed for Al/NMC and Al/poly/NMC samples to determine the quality of cell protection. The tests included single charging to the upper voltage value of 8.0 V at 0.1C followed by recording of chronoamperometric response of the cells at 8.0 V. The cells were also recharged several times within the 2.8−5.0 V voltage range at a current rate of 0.1C to determine the efficacy of polymer layer protection under the expanded voltage range. All the stress test measurements were preceded and followed by recording the EIS and CV data.

External short circuit tests were performed by setting a 0.0 V voltage between positive and negative terminals of the cells and recording the current response for 1800 s. The experiments were preceded and followed by recording of GCD and CV data.

Material Characterization. After the cells were overcharged with both protected Al/poly/NMC and unprotected Al/NMC electrodes, the batteries were disassembled, and the cathodes were extracted. The cathodes were thoroughly rinsed with acetonitrile to remove the excess of the electrolyte and dried. The extracted cathodes as well as pristine electrodes (not participating in any electrochemical tests) serving as reference samples were then characterized with the following methods.

The X-ray photoelectron spectra (XPS) were recorded on a Thermo Fisher Escalab 250Xi with nonmonochromated Al K_α radiation (photon energy 1486.6 eV) and total energy resolution of ca. 0.3 eV. The spectra were obtained at room temperature under an ultrahigh vacuum of ca. 1×10^{-9} mbar. Constant pass energy mode at 20 eV was used, with a 650 μm diameter analysis area. For data processing, binding energy values were referenced to the C 1s peak (284.8 eV) from the adventitious contamination layer.

Scanning electron microscopy (SEM) and energy-dispersive X-ray spectroscopy (EDX) studies were performed by using a Zeiss Merlin microscope.

XRD spectra of the samples both before and after cycling were obtained using a Bruker-AXS D8 DISCOVER diffractometer with a Cu K_α source (λ = 1.5418 Å) in the 15−90° range. The phases were identified using the *PDF-2 ICDD Release 2016* powder diffraction database and PDXL2 v2.7.2.0 software.

The data were plotted using OriginPro (≥9.0) software, and SEM/EDX images were tinted and overlaid using GIMP 2.10.30 software. Scientific color map *batlow*[35] was used to prevent visual distortion of the data.

RESULTS AND DISCUSSION

The primary target when designing the internal resistance switch for NMC-based cells was to trigger the resistance increase of the protective layer before reaching the destructive voltage value while minimizing the polymeric layer-induced voltage loss in the cell under normal operational conditions.

The working potential range of NMC cathodes of 2.8−4.2 V[28,36] matches well the conductivity window of poly[Ni(CH_3OSalen)]. The polymer is conductive at 3.0−4.2 V, while at 4.2 V, a reversible switching to the nonconductive state

https://doi.org/10.1021/acsaem.3c02145
ACS Appl. Energy Mater. XXXX, XXX, XXX−XXX

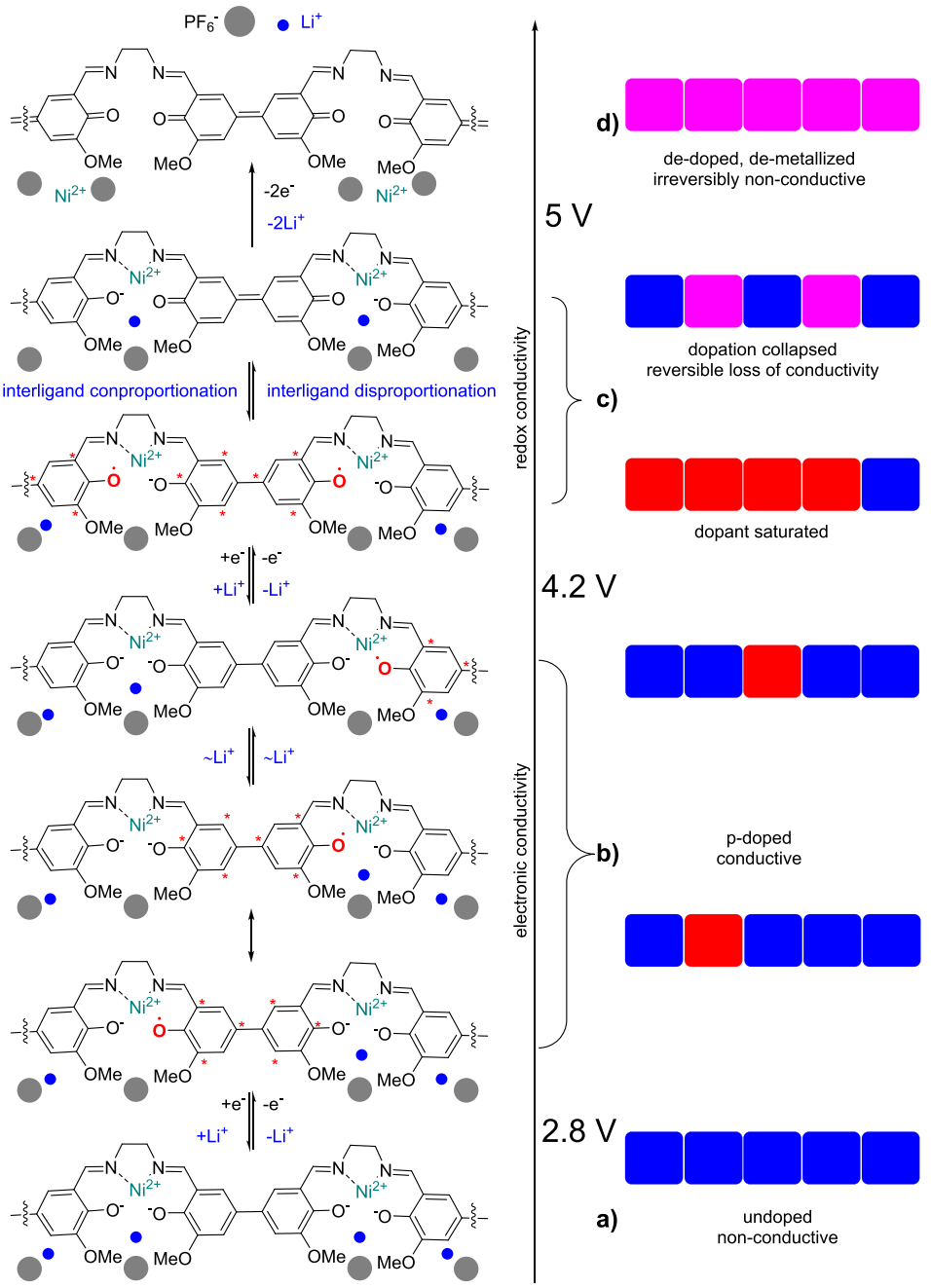

Figure 1. Mechanistic scheme of the potential-dependent resistivity of poly-[Ni(CH_3Osalen)] underlying the protective effect of the poly-[Ni(CH_3Osalen)] layer in NMC-based cells. (a) Undoped nonconducting state at voltages below 2.8 V; (b) p-doped semiquinoid redox conducting state at voltages between 2.8 and 4.2 V with electronic conductivity; (c) dopant-saturated semiquinoid state between 4.2 and 5 V with low-level redox conductivity; (d) dedoped, demetallized, and probably partly decomposed quinoid state with irreversible loss of conductivity above 5 V. To facilitate the discussion, the covalent Ni−O bond is depicted as ionic pair, see text for details.

occurs, which withstands potentials up to 5.0 V. Above 5.0 V, the polymer loses conductivity irreversibly.[30] At the molecular level, the potential-dependent conductivity of poly[Ni-(CH_3Osalen)] can be rationalized as transformation from nonconductive phenolate through conductive semiquinoid to the nonconductive quinoid forms of the ligand (Figure 1). At a voltage below 2.8 V, the polymer is in neutral form with occasional inclusion of both electrolyte cations and anions, Li^+ and PF_6^-, in balanced proportions. The ligand can be described as a phenolate form at this stage (Figure 1a). With increased voltage, the polymer is oxidized and turns to a p-doped conductive state. The ligand at this stage attains semiquinoid radical-anion character, and the medium becomes depleted with Li^+ cations within the polymer matrix (Figure 1b).[37] An additional increase in potential results in an increased concentration of "holes" (compensated with subsequent depletion with Li^+), leading to increased conductivity until it reaches a maximum at some potential corresponding to the optimal ratio of doped and undoped polymer molecules. At a potential of 4.2 V, the polymer becomes dopant-saturated, that is, the ratio of doped and undoped molecules becomes distorted in favor of oxidized polymer molecules. The ligands in the polymer at this stage are equilibrated between the chain of semiquinoid structures and

https://doi.org/10.1021/acsaem.3c02145
ACS Appl. Energy Mater. XXXX, XXX, XXX−XXX

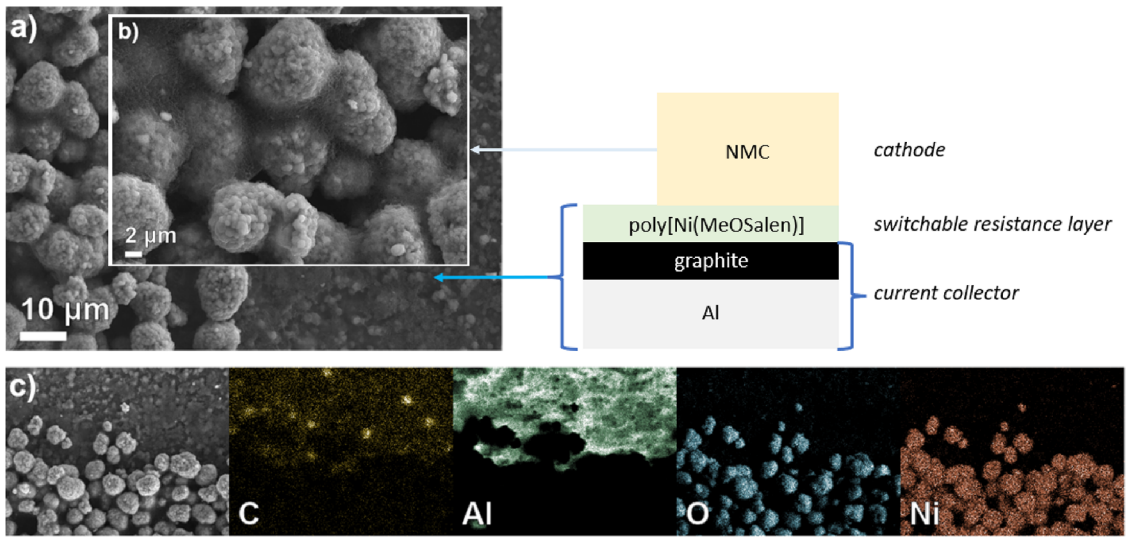

Figure 2. (a) SEM image of the edge of the NMC coating on top of the polymeric layer in the Al/poly/NMC sample, (b) SEM image of the NMC within the coating at a higher magnification, and (c) fragment of the coating with both NMC and bare poly[Ni(CH_3OSalen)] film visible along with the EDX mapping of elements in the presented area.

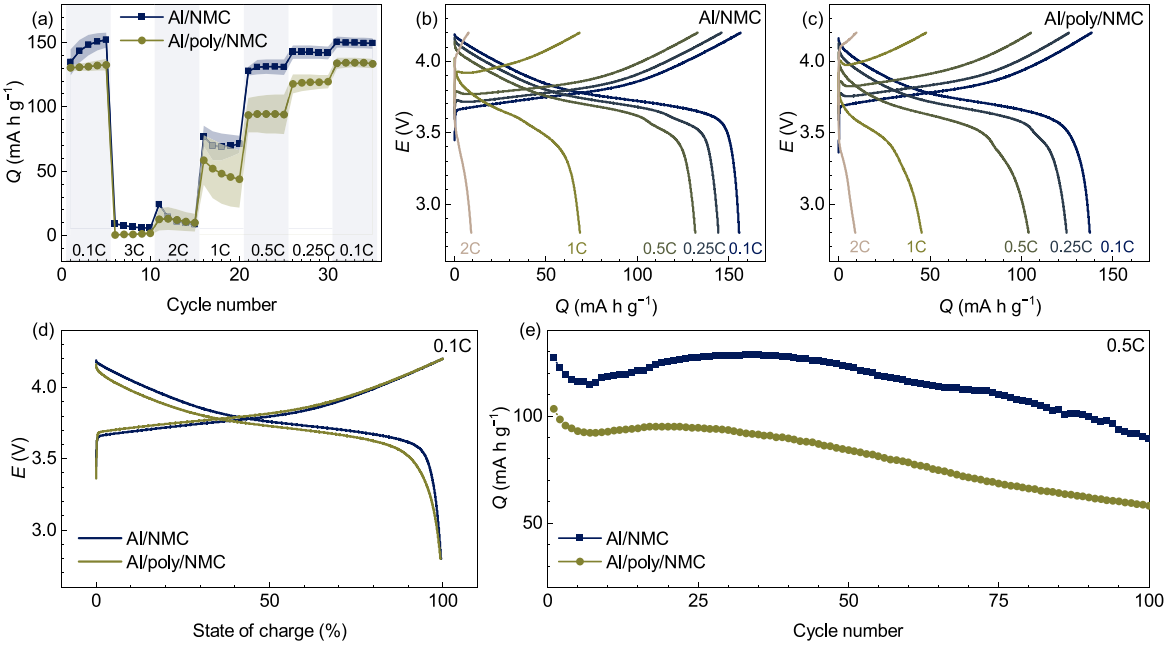

Figure 3. (a) C-rate capability of protected and unprotected NMC electrodes, GCD curves of electrodes at various current rates for (b) Al/NMC and (c) Al/poly/NMC electrodes, (d) GCDs at 0.1C in potential vs state-of-charge coordinates, and (e) cycling stability of electrodes at 0.5C.

phenolate-quinoid pairs (Figure 1c) in a disproportionation/conproportionation equilibrium. While expansion of π-conjugation through nickel ions is feasible for semiquinoid ligands, affording thus intrachain electronic conductivity in doped poly[Ni(CH_3Osalen)], such conjugation is hardly possible with quinoid ligands as the Ni−O bonding interaction becomes orthogonal to the π-orbitals of the quinoid ligand. Hence, the electron transport switches to the redox mechanism, affording a much lower conductivity. Above 5 V, the ligands are in the quinoid state only (Figure 1d), depleted of Li^+, showing zero or very low intrinsic conductivity. Most probably, the polymer at this state becomes demetallized and chemically degraded. Thus, the poly[Ni(CH_3Osalen)] layer would serve as a conducting interface under the normal operational conditions of the cell, yet it would switch to a nonconducting state upon overcharging or overdischarging.

As poly[Ni(CH_3Osalen)] can be easily electrodeposited on a conductive surface,[34] we coated graphitized aluminum foil, the future current collector, with a poly[Ni(CH_3Osalen)] film by electropolymerization of the monomeric precursor, [Ni(CH_3Osalen)]. The deposition was charge-controlled to reproduce the optimal polymer layer parameters reported in our previous studies on $LiFePO_4$ cathodes (i.e., 0.05 V drop in achievable cell voltage and 16 times resistance increase at overcharge).[30] The thickness of the polymer film was estimated to be ca. 1 μm according to coulometric data as described previously.[38] NMC/carbon black/PVDF slurry in *N*-methylpyrrolidone was cast then over the poly[Ni(CH_3Osalen)] layer, producing a "sandwich" electrode,

https://doi.org/10.1021/acsaem.3c02145
ACS Appl. Energy Mater. XXXX, XXX, XXX−XXX

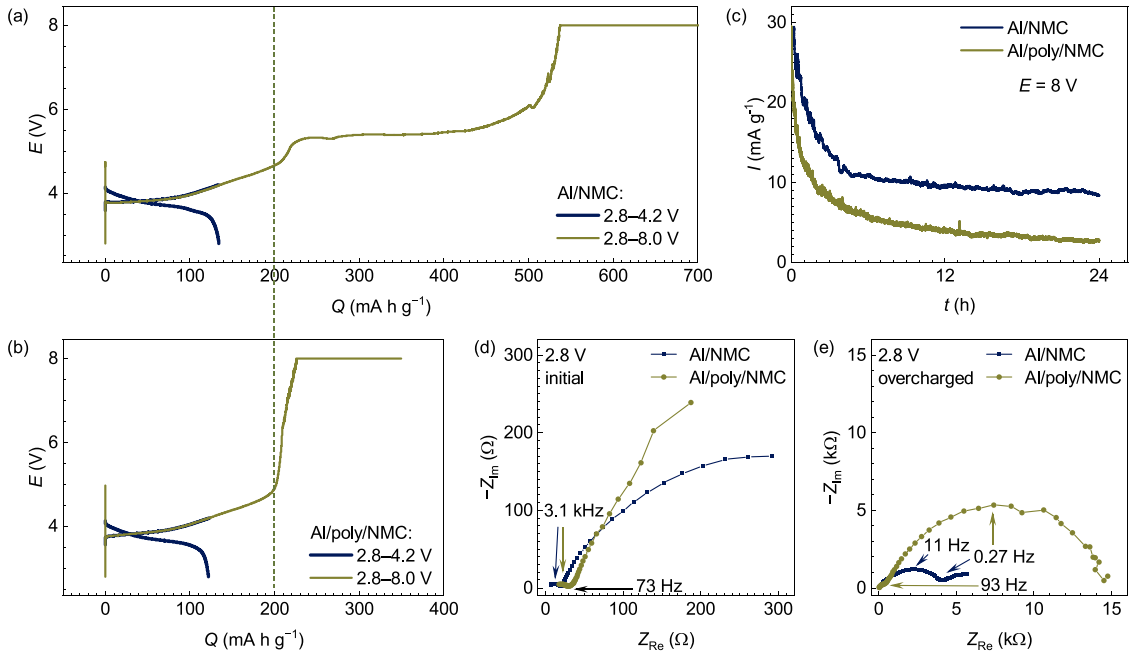

Figure 4. CCCV curves at 0.1C within the operational voltage window (2.8−4.2 V) and upon overcharging to 8.0 V for (a) Al/NMC and (b) Al/poly/NMC; (c) potentiostatic response of the materials at E = 8.0 V; EIS spectra of Al/NMC and Al/poly/NMC (d) in the discharged state (2.8 V) after cycling in normal cycling conditions and (e) after achieving the overcharged state.

where active mass was separated from the current collector by a switchable-resistance layer (Figure 2).

The SEM image of the polymer-protected Al/poly/NMC sample (Figure 2a) shows a typical globular morphology of NMC coating[27,39] with small (ca. 100 nm in diameter) granules bunched up to larger (ca. 10 μm in diameter) globules (Figure 2b). At the electrode surface free of NMC coating, the granular surface of the protective poly[Ni(CH_3Osalen)]layer can be seen (Figure 2a, the blue arrow), similar to the pattern reported before.[40]

The EDX elemental mapping (Figure 2c) confirms the expected composition of the NMC layer (Ni, O, also Mn, Co, see Figure S1), while the protective polymer layer proves to be thin enough to show the graphitized aluminum substrate beneath, as the penetration depth of the EDX method with 20 keV primary electron beam would be approximately 3−10 μm, according to the Anderson & Hasler equation.[41]

The capacity of the NMC cathode in protected and unprotected samples was estimated from standard GCD tests. The highest capacity of the material on the unprotected electrode, Al/NMC, is 152 mA h g^{-1} at 0.1C (Figure 3a). This value is close to the commonly reported specific capacity of 160 mA h g^{-1} for NMC,[42,43] and the slight decrease originates most likely from the increased ohmic resistance within the material caused by the excessive mass loading of 40 mg cm^{-2}. The protected electrode, Al/poly/NMC, provides a slightly lower value of 133 mA h g^{-1}. The reason for this capacity decrease is most probably the additional ohmic-induced voltage drop (IR drop) within the polymer layer. In the following sets of cycles at various current rates (Figure 3a), the minimum capacity was observed at 3C. The capacity values at 3C and 2C do not exceed 24 mA h g^{-1} even in the case of the unprotected electrode, which indicates that fast recharging rates are unavailable for this load (40 mg cm^{-2}) of NMC material. At 1C, 0.5C, and 0.25C, Al/poly/NMC demonstrates up to 59, 94, and 120 mA h g^{-1}, respectively. The capacity loss of Al/poly/NMC as compared to Al/NMC increases along with the current rate: the samples lose only ca. 10% of capacity at 0.1C, while at 1C, up to 25% is lost. This agrees well with the IR drop in both the polymer layer and cathode material loaded at 40 mg cm^{-2} that implies monotonic growth of the voltage drop along with current increase. The effect of the polymer on the charge−discharge polarization and the main discharge plateau potential is thus insignificant at currents up to 0.25C. At such current rates, the mean potential value is ca. 3.8 V, but it drops slightly as the current density increases (Figure 3b,c).

The shape of the GCD suffers minimal changes upon addition of the protective layer (Figure 3d). This shows that the protective layer remains conductive under normal operational conditions of the cathode material.

However, the protective layer reduced the durability of the cells (Figure 3e). After 100 cycles, Al/NMC electrodes keep 71% of the initial capacity value, while the Al/poly/NMC electrode retains only 56%. We believe this shortcoming to stem from the degradation of the protective layer interface upon prolonged cycling.

To study the protective efficacy of the polymer layer against overoxidation, we performed a series of stress tests on the cells: overoxidation to 8 V, overoxidation to 5 V, and short circuit conditions.

Modeling a sharp potential increase event, we recorded the current response of the protected and unprotected cells toward an applied constant potential of 8 V (Figure 4c). The current response of the unprotected Al/poly/NMC cell plateaued at ca. 8.5−10 mA g^{-1}, implying that electrochemical reactions continue to proceed in the overoxidized cell and put the cell to the risk of ignition. On the contrary, the protected Al/poly/NMC cell decays to a much lower value of 2.5−3.5 mA g^{-1}, implying that the addition of poly[Ni(MeOSalen)] minimizes the intensity of adverse processes and renders the cell nonconductive upon strong overoxidation.

https://doi.org/10.1021/acsaem.3c02145
ACS Appl. Energy Mater. XXXX, XXX, XXX−XXX

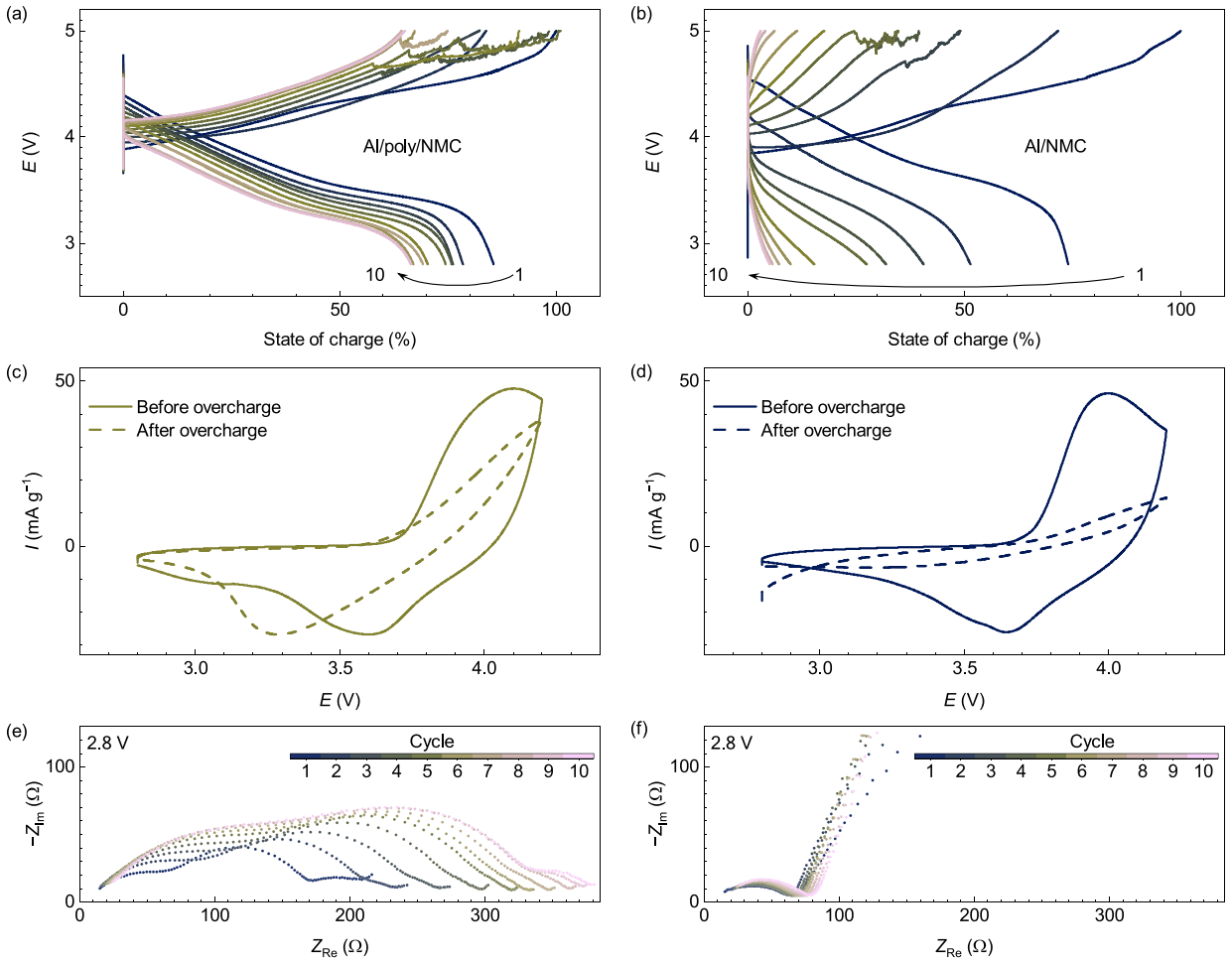

Figure 5. GCD curves of 10 consecutive cycles at 0.1C within the expanded potential window (2.8−5.0 V) for (a) Al/poly/NMC and (b) Al/NMC; CVs of (c) Al/poly/NMC and (d) Al/NMC prior to and after cycling the cells within the expanded potential window; EIS of the cells with (e) Al/poly/NMC and (f) Al/NMC materials after each GCD cycle in the expanded potential window.

In a series of CCCV (constant current−constant voltage charging) measurements of overcharging response of the cells, we collected information on separate steps of the bulk deterioration process. Within these experiments, the samples were charged by constant current until a potential of 8.0 V was reached followed by potentiostatic charging at this potential (Figure 4a,b).

The constant current part of the CCCV response of the unprotected Al/NMC sample shows two levels of relatively constant potential, which correspond to nondestructive cell charging at 0−4.7 V followed by cell degradation at 4.7−8.0 V (Figure 4a), implying two-step oxidation of the cell material. The charge passed through the cell in constant current mode exceeded the nominal capacity value by ca. 300%, indicating the occurrence of some destructive redox processes upon overcharging. The CCCV response of the protected sample (Figure 4b) differs drastically as only one potential level is observed before the sharp potential rise to the upper limit, which suggests dramatic resistance changes in the material instead of two-step oxidative degradation. The total capacity gained in the constant current mode exceeded the nominal value only by 185%, showing the yield of the undesirable processes in the cell to be significantly lower as compared to the unprotected cell.

Careful examination of the CCCV responses shows that the excessive "capacity" of the unprotected cell is gained between 5.3 and 5.7 V, and this capacity gain step is absent in the protected Al/poly/NMC sample. These potential values correspond to decomposition of carbonate-based electrolyte EC:DEC,[29,44] which could be the reason for the jagged and irregular shape of CCCV response of the unprotected sample at the 5.7−8.0 V range. The protected sample shows a monotonous potential rise in this range. From these data, we conclude that the polymeric layer eliminates the decomposition of the electrolyte and prevents the thermal runaway of the cell by transitioning to the nonconductive state upon overcharging of the cell.

The experiments on overcharging to 8.0 V showed that the protective polymer layer reduces the current flow through the cell almost to zero when the cell is placed under extreme conditions, typically leading to hazardous cell deterioration. As a result, the cell becomes inoperative, yet it remains safe. To explore the overcharge protective efficacy of the polymer layer with regard to the cell operability, we overcharged the cells to 5.0 V, which is the upper limit of the range of reversible nonconductivity of poly[Ni(CH_3Osalen)].

Repeated overcharging of the Al/poly/NMC cells with the poly[Ni(CH_3Osalen)]-protected electrode to 5.0 V led to only 22% loss of discharge capacity over 10 cycles (Figure 5a), as

https://doi.org/10.1021/acsaem.3c02145
ACS Appl. Energy Mater. XXXX, XXX, XXX−XXX

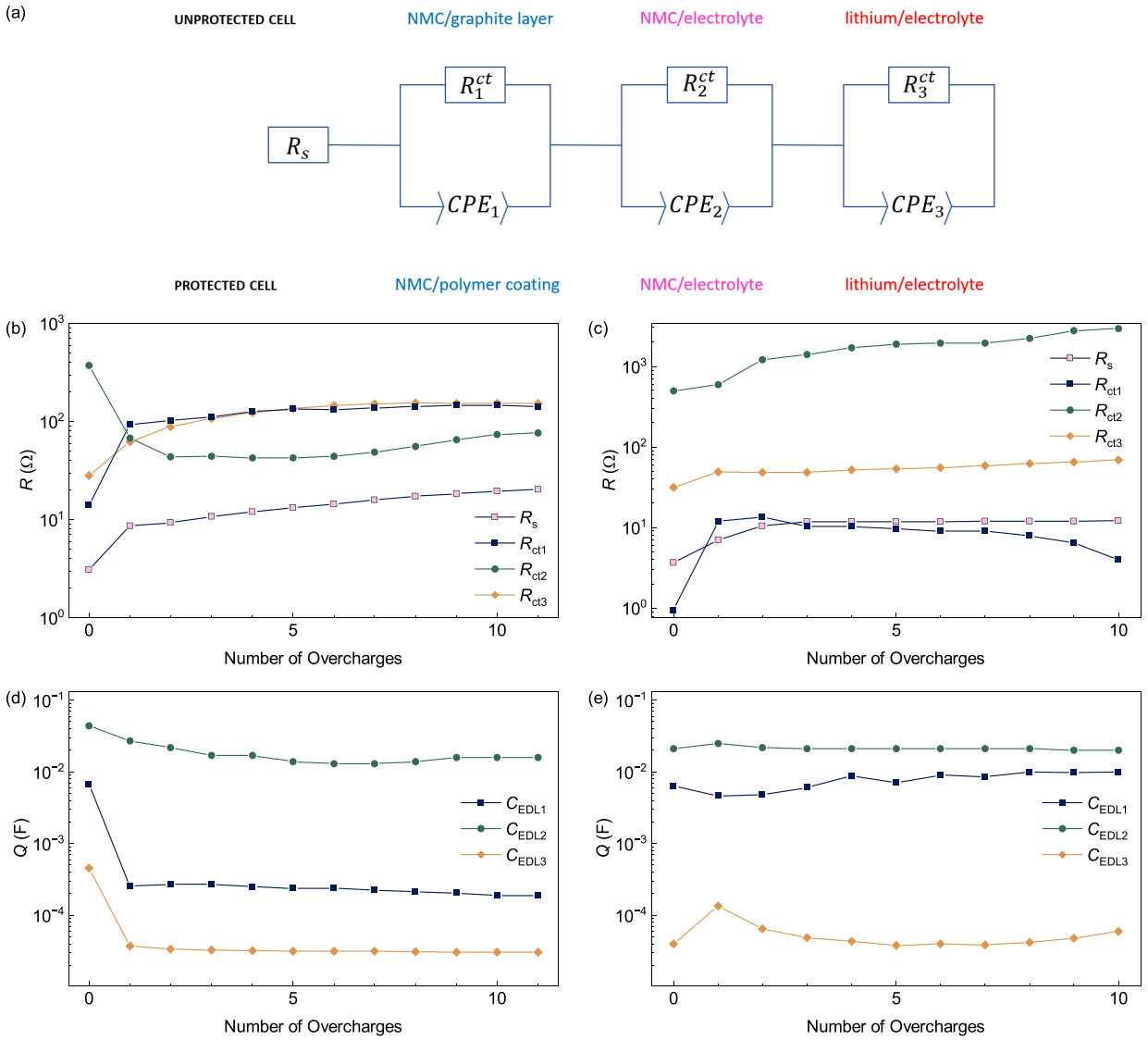

Figure 6. (a) Equivalent circuit model for protected (Al/poly/NMC) and unprotected (Al/NMC) cells (top) and evolution of the model parameters (R_{ct} and CPE) during operation of (b and d) protected and (c and e) unprotected cells.

compared to the unprotected Al/NMC cell (Figure 5b) that lost its capacity entirely, providing no more than 74% of the initial Coulombic efficiency and yielding only 4% of the initial discharge capacity by the 10th cycle. The dramatic decrease in Coulombic efficiency of the unprotected cell can be caused by both NMC degradation[28] and $LiPF_6$ decomposition[29] at higher potential values.

As for the protected cell, expanding the potential window to 5.0 V decreases the initial Coulombic efficiency to 85% as compared to that under normal operation conditions. This 15% capacity loss is most probably caused by the decomposition of $LiPF_6$ incorporated in the poly[Ni-(CH_3Osalen)] matrix. The potential drop at high voltages is mostly localized within the polymer layer due to the nonlinear resistivity response of the latter. For this reason, the NMC cathode material remains outside the area of damaging voltage, while $LiPF_6$ is partly affected by the harsh conditions. As long as the polymer matrix remains undamaged, both Li^+ and PF_6^- ions can transport freely between the bulk mass of the cathode material and the polymer layer to substitute for the decomposed PF_6^- anions. This explains lower capacity losses per 10 cycles of the protected cell at 5 V as compared to unprotected cell (22% vs 96%, respectively). Though the observed capacity loss is non-negligible, the protected cell remains functionable after such impact, which is an unprecedented achievement for polymer-protected electrodes and a valuable advantage over protection through irreversible polymer overoxidation as reported for poly(3-butylthiophene).[32]

The retention of the electrochemical activity of the Al/poly/NMC cell after overcharging to 5.0 V was also evident in cyclic voltammetry measurements. While the cyclic voltammogram of the unprotected Al/NMC cell (Figure 5d) degrades completely after overcharging to the point of negligible electrochemical response, the protected Al/poly/NMC cell retains distinct redox peaks, though the postovercharging cyclic voltammogram becomes skewed (Figure 5c), and the major peak separation increases.

The difference in resistance pattern as the origin of different responses to overcharge in protected and unprotected electrodes is corroborated by EIS measurements (Figure 5e,f). Impedance spectra of both cells were fitted with an

https://doi.org/10.1021/acsaem.3c02145
ACS Appl. Energy Mater. XXXX, XXX, XXX−XXX

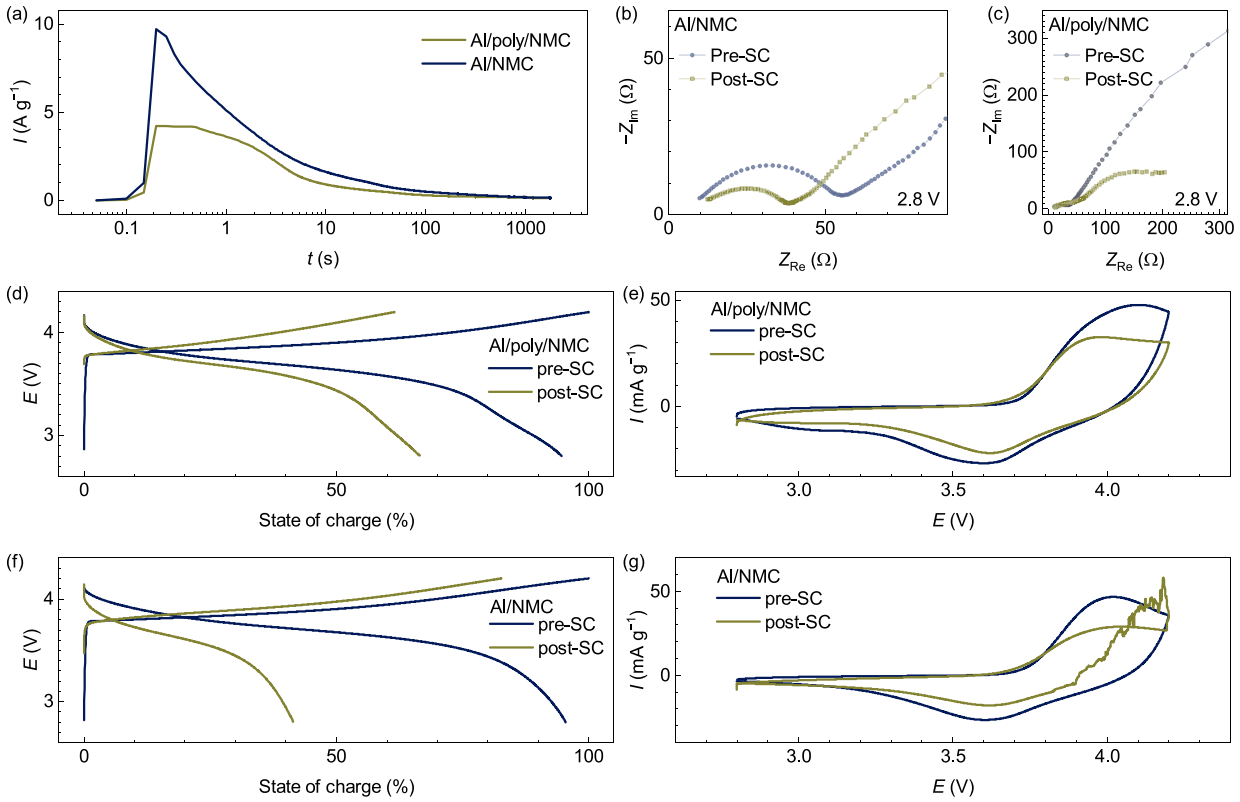

Figure 7. (a) Current response upon short-circuiting (SC) the cells with and without the protective NMC layer; EIS of the cells with (b) Al/NMC and (c) Al/poly/NMC electrodes before and after the short-circuiting; comparison of (d, f) GCD and (e, g) CV response of the cells with (d, e) Al/poly/NMC and (f, g) Al/NMC materials prior to and after the short-circuiting.

equivalent circuit, consisting of a series of three R/CPE circuits, reflecting charge transfer at three interfaces: NMC/electrolyte, polymer/NMC or graphite//NMC, and electrolyte/lithium anode interfaces (Figure 6a), which is typical of NMC/Li cells.[45,46]

Under normal operation conditions (2.8 and 4.2 V), both cells demonstrate quite similar impedance patterns. The R/CPE component of the lowest capacitance (10^{-4}–10^{-5} F) and intermediate resistance (ca. 30 Ω) can be attributed to the injection of lithium ions and charging of the double electric layer at the lithium anode/electrolyte interface, which is expected to have flat boundary of small area and hence small capacitance. The components of the highest capacitance (2–5 × 10^{-2} F) and highest resistance (400–500 Ω) can be attributed to the NMC/electrolyte interface, which has the largest boundary area. The R/CPE component of intermediate capacity (6–7 × 10^{-3} F) and low resistance can be attributed to the NMC/carbon (1 Ω) interface in the unprotected cell and to the NMC/polymer (15 Ω) interface in the protected cell. Thus, insertion of the polymer layer between graphitized aluminum and NMC expectedly increases the charge transfer resistance.

A series of successive overcharges (galvanostatic charge 1C up to 5 V) impacts differently the protected and unprotected cells. Thus, the overall resistance ($R_s + R_{ct1} + R_{ct2} + R_{ct3}$) of the unprotected cell grows fast with each new overcharge cycle, giving a 6-fold increase from ∼0.5 kΩ to ∼3 kΩ by the 10th cycle, while the overall resistance of the protected cell remains nearly the same (around 450 Ω). Deconvolution of the overall impedance response to individual components revealed that this difference was due to the polymer insert. While the anode/electrolyte interface shows roughly the same behavior in both protected and unprotected cells (Figure 6b,c, hollow squares), the NMC-associated interfaces differ dramatically. The resistance of the NMC/electrolyte interface steadily grows from 500 to 3000 Ω for the unprotected material, while it remains within the range of 40–70 Ω after the initial drop from 400 to 70 Ω for the polymer-protected material. In the protected cell, a polymer/NMC interface is developed, with a new resistance component rising fast from 10 to 100 Ω during the first cycle and remaining close to this value thereafter.

Overcharging to 8 V also produces a different response in protected and unprotected cells. While the unprotected cell shows ca. 1–2 orders of magnitude increase in R_{ct} across all interfaces (Figure 4d,e), the protected cell demonstrates only moderate changes in charge transfer resistance across NMC/electrolyte and anode/electrolyte interfaces along with a sharp increase to 15 kΩ in the resistance across the poly/NMC interface (R_{ct1}). Hence, we conclude that a high-voltage overcharge (up to 8 V) results in a significant decrease in the conductivity of the polymer layer.

Based on these results and the known instability of NMC materials above 4.4–4.6 V (for any Ni:Mn:Co ratio)[47] and reversible resistance increase in poly[Ni(CH_3Osalen)],[33] we conclude that the observed increase in the resistance for unprotected cell upon overoxidation, to either 5 or 8 V, is caused by both the degradation of the NMC material and decomposition of the electrolyte. In the protected cell, a fast rise in the resistance of the polymer/NMC interface decreases the effective potential at the polymer/NMC boundary and prevents overoxidation of the cathode material.

https://doi.org/10.1021/acsaem.3c02145
ACS Appl. Energy Mater. XXXX, XXX, XXX−XXX

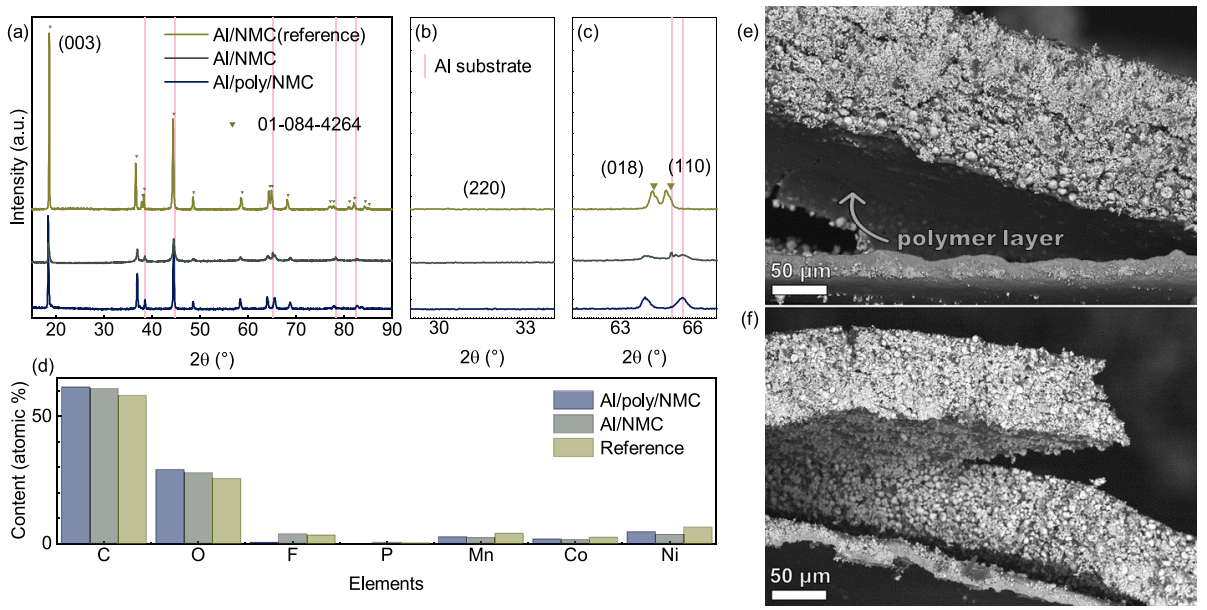

Figure 8. (a) XRD spectrum of Al/NMC and Al/poly/NMC electrode samples after overcharging, with the Al/NMC electrode (unaffected by electrochemical studies) for reference; (b, c) magnified areas of the XRD spectra in specific regions; (d) elemental composition of samples according to EDX data of samples; and SEM images of (e) Al/poly/NMC and (f) Al/NMC samples.

Another important problem is the cell defense in case of short-circuiting events, which usually affects all three components of the electrochemical system: cathode, anode, and electrolyte.[48,49]

We compared the effects of external short-circuiting on the cells with either a protected or unprotected cathode. When the external potential between the cathode and anode was set to 0.0 V, the cells showed a rapid (within 0.2 s) increase in current density to 9.7 A g^{-1} (69C) for Al/NMC and 4.2 A g^{-1} (30C) for Al/poly/NMC (Figure 7a). The current densities relaxed to 1−2 A g^{-1} (7−14C) within ∼10 s and reached ∼0.2 A g^{-1} (1.4C) after 1000 s. Though the relaxation times of both samples were close, the protected sample demonstrated lower peak currents and admitted a lower amount of charge to pass through the cell. The cutoff response of the polymer-protected cell indicates the beginning of several consecutive processes affecting the cell resistivity, while the sharp response of the unprotected cell indicates the existence of one major process.

The noncomplete degradation of the protective layer is evident from the GCD (Figure 7d) and CV (Figure 7e) response for Al/poly/NMC cells. The cell retains 69% of its initial discharge capacity after the short circuit testing procedure. Similarly, the shape of CV remains the same after the test, though there is a slight drop in the current density. Thus, the intermediate layer of the polymer with switchable conductivity allows us to protect all components of the cell upon abuse.

Conversely, the short-circuiting causes the unprotected Al/NMC cells to retain only 43% of the initial discharge capacity in subsequent charging (Figure 7f), and the ongoing degradation processes result in a meager 50% Coulombic efficiency. As the jagged response in CVs (Figure 7g) shows, the degradation occurs from 3.9 V upward, which may include interaction of either of the components of the cell, as a lack of protective layer allows free flow of the current across both the cathode/electrolyte and anode/electrolyte interface.

To understand the changes occurring in the material, both the protected, Al/poly/NMC, and unprotected, Al/NMC, cells were disassembled after overcharging to 8.0 V, the maximal potential studied in this work, and the extracted cathodes were studied with XRD, SEM/EDX, and XPS methods.

According to previous reports,[50,51] thermal decomposition of the NMC-cathode during the thermal runaway process is accompanied by the transformation of the material from the initial layered structure to disordered $LiMn_2O_4$-type spinel, indicated by the disappearance of the peak at 18.6° ((003) plane) and emergence of the (220) peak at ∼31° and peaks for (440) or (200) planes at 61−67° range.[51] This is not the case in our study (Figure 8a−c). Regardless of the presence of the protective polymeric layer, the XRD spectra (Figure 8a) of samples correspond to the $Li(Mn_{0.30}Co_{0.20}Ni_{0.50})_2O_2$ structure (ICDD 01-084-4264) with an *R*3*m* space group and trigonal crystal system. Careful inspection of the 61−67° range (Figure 8c) shows only widening of the gap between (018) and (110) peaks, indicating the additional charging of the overcharged material compared to the reference sample, where these peaks are positioned more tightly.[52,53]

According to EDX (Figure 8d), the ratio of Ni, Mn, and Co atoms in the active materials comprises 5:3:2 and it remains constant for all the samples (reference, overcharged protected, and overcharged unprotected cathodes). As compared to the reference and to the protected cathode samples, the unprotected electrode extracted from the overcharged cell have higher contents of F, C, and P atoms arising from either electrolyte decomposition or SEI formation. The decomposition of the electrolyte may proceed through oxygen release, which is known to accompany NMC cathode material overcharging processes.[47] The oxygen released upon oxidation of the cathode material reacts with the electrolyte and accumulates additional C in the cathode material. As a result, the C/Ni ratio in the unprotected sample increases to 17:1 from 9:1 in the protected sample and 13:1 in the reference one. Such difference additionally confirms the overcharge-protective properties of poly[Ni(CH_3OSalen)].

The images of Al/NMC and Al/poly/NMC samples (Figure 8e,f) reveal the drastically different morphological properties of

https://doi.org/10.1021/acsaem.3c02145
ACS Appl. Energy Mater. XXXX, XXX, XXX−XXX

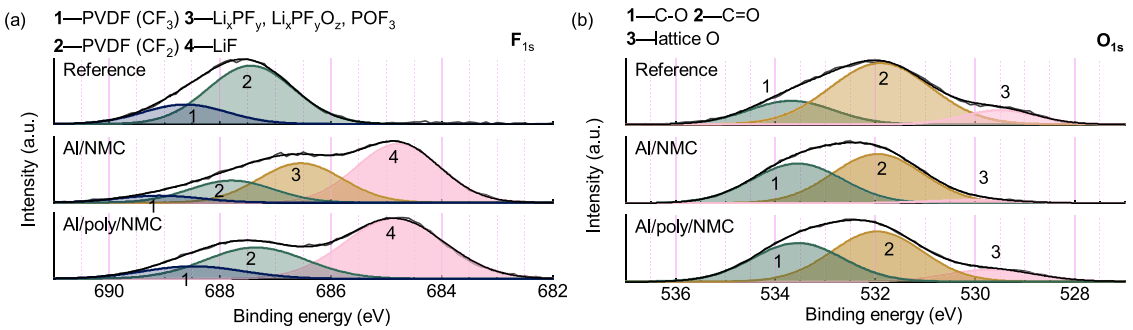

Figure 9. Deconvolution of (a) F 1s and (b) O 1s spectra of Al/NMC, Al/poly/NMC, and reference samples.

the foil-facing side sample coating. The coatings were separated from the substrate to show the contact surface. The unprotected electrode material has the same rough and crumbly morphology from the side of the foil as it does from the edge, i.e., the bulk of the material is permeable and in direct contact with the graphitized foil. In contrast, the protected sample has a smooth and uniform surface formed by the polymer layer from the side of the coating that touches the aluminum foil. The aluminum foil surface also does not contain any crumbs of NMC electrode material, which is not the case for the unprotected sample. Thus, the continuous layer should provide reasonable overcharge protection in further electrochemical tests.

The XPS spectra of the electrode surface were recorded for protected Al/poly/NMC and unprotected Al/NMC samples subjected to overoxidation at 8 V and compared to the uncycled reference (Figure 9).

The F 1s spectrum (Figure 9a) of the reference sample contains two peaks at 687.4 eV (**2**) and 688.6 eV (**1**) of CF_2 and CF_3 of the PVDF binder, respectively. The spectra of Al/NMC and Al/poly/NMC transform notably: an F^- peak at 684.8 eV (**4**) emerges for both overcharged samples, which is related to LiF deposited on the electrode due to electrolyte decomposition.[54] In addition, a peak at 686.6 eV (**3**) appears in Al/NMC, which corresponds to fluorine bound to phosphorus and is thus indicative of the substantial presence of electrolyte decomposition products like Li_xPF_y, $Li_xPF_yO_z$, and POF_3.[55−57]

For all samples, the O 1s spectra (Figure 9b) contain peaks at 533.2 eV (**1**) and 531.7 eV (**2**) that correspond to O^{sp3} and O^{sp2} in C−O[58] and C=O[54,59] bonds, respectively, in the conducting additive, arising from carboxyl or carbonyl groups present in the carbon material. The peak at 529.5 eV (**3**) is pertaining to oxygen within the NMC crystal lattice.[54,60] This peak is present in both reference and Al/poly/NMC samples but is absent in unprotected Al/NMC, indicating pulverization of the material upon overcharging of the unprotected electrode.

The Mn 2p spectra and Co 2p spectra (Figures S2 and S3) are similar for all samples and show typical of NMC pattern[61−64] with signals at 642.1 eV (Mn $2p_{3/2}$), ~653−654 eV (Mn $2p_{1/2}$), 780.2 eV (Co $2p_{3/2}$), and 795.4 eV (Co $2p_{1/2}$). The Ni 2p spectra of all samples also demonstrate characteristic Ni 2p signals as 2:1 doublet due to spin−orbit splitting in core-ionized ions, with Ni $2p_{3/2}$ and Ni $2p_{1/2}$ components centered around ca. 858 and 876 eV, respectively (Figure S4). However, the fine structure of the components in the Ni 2p spectra differs notably across these samples. While the reference sample shows typical for NMC material spectrum[63,64] with main lines at ca. 855.0 eV (Ni $2p_{3/2}$) and 872.7 eV (Ni $2p_{1/2}$) accompanied by shake-down satellites, the unprotected cathode material Al/NMC subjected to 8 V voltage demonstrates ca. 2 eV shift of the most intense lines to ca. 857.2 and 875.8 eV, respectively. Within the Gupta and Sen model for fine structures of XPS multiplets due to spin−orbital coupling,[65] the intensity of high energy components (+2−3 eV) increases in the envelope for Ni^{3+} multiplet as compared to the envelope for Ni^{2+} multiplet. These data thus indicate a significant presence of Ni^{3+} in the overoxidized unprotected cathode material. A comparison of Ni $2p_{3/2}$ spectra of Al/NMC and γ-$Ni^{III}OOH$[66] suggests that Al/NMC contains ca. 20% of Ni^{2+} along with Ni^{3+} as Ni^{3+} alone cannot explain such signal broadening. The Ni 2p spectrum of the polymer-protected cathode material Al/poly/NMC is well approximated by a linear combination of the Ni 2p spectra of the reference and Al/NMC samples in a 0.6:1.1 ratio (Figure 10). In view of the above analysis, this gives a ca. 1:1 Ni^{2+}/Ni^{3+} ratio in the protected material as compared to a ca. 1:4 Ni^{2+}/Ni^{3+} ratio in the unprotected material.

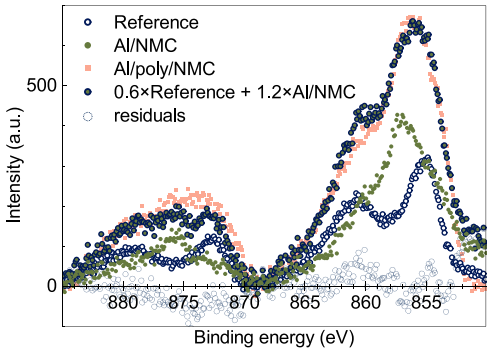

Figure 10. Ni 2p spectra of the reference sample, Al/NMC, and Al/poly/NMC imposed to approximation of Ni 2p spectrum of Al/poly/NMC as a linear combination of the Al/NMC and reference sample spectra.

Thus, overoxidation of the unprotected Al/NMC cathode results in PVDF binder oxidation and pulverization of the crystalline lattice due to oxidation of Ni^{2+} to Ni^{3+}. Insertion of the poly[Ni(MeOSalen)] protective layer between the current collector and cathode material protects the PVDF binder from oxidation and endows ca. 30% reduction in oxidation of the NMC cathode material, which is sufficient to prevent crystalline lattice pulverization.

https://doi.org/10.1021/acsaem.3c02145
ACS Appl. Energy Mater. XXXX, XXX, XXX−XXX

CONCLUSIONS

The poly[Ni(CH_3Osalen)] protective layer electrochemically deposited between the current collector and active cathode material effectively prevents hazardous decomposition of the cell components in NMC532 lithium-ion batteries. The polymer layer remains conductive within the safe potential range of 3.0−4.2 V but transitions to a nonconductive state upon overcharge to 5.0 V or external short circuit events. This switch limits current flow and protects internal components from degradation. The reversible switching process maintains a significant portion of the cell capacity over multiple cycles. Cells with NMC cathodes protected by the poly[Ni-(CH_3Osalen)] layer retain up to 87.5% of the capacity value of unprotected samples, providing a reasonable compromise between the battery performance and safety. Overcharging of the cell to 8.0 V results in an irreversible transition of the polymer to a nonconductive state, thus creating an insulator layer within the cell and reducing the risk of further material degradation, flammable gas release, and combustion.

ASSOCIATED CONTENT

Supporting Information

The Supporting Information is available free of charge at https://pubs.acs.org/doi/10.1021/acsaem.3c02145.

SEM, EDX, and XPS of samples (PDF)

AUTHOR INFORMATION

Corresponding Author

Oleg V. Levin − *Institute of Chemistry, St. Petersburg University, St Peterburg 199034, Russian Federation;* orcid.org/0000-0002-4538-316X; Email: o.levin@spbu.ru

Authors

Evgenii V. Beletskii − *Institute of Chemistry, St. Petersburg University, St Peterburg 199034, Russian Federation*

Alexey I. Volkov − *Institute of Chemistry, St. Petersburg University, St Peterburg 199034, Russian Federation;* orcid.org/0000-0002-8113-2595

Elena V. Alekseeva − *Institute of Chemistry, St. Petersburg University, St Peterburg 199034, Russian Federation*

Dmitrii V. Anishchenko − *Institute of Chemistry, St. Petersburg University, St Peterburg 199034, Russian Federation;* orcid.org/0000-0003-4093-0475

Alexander S. Konev − *Institute of Chemistry, St. Petersburg University, St Peterburg 199034, Russian Federation;* orcid.org/0000-0003-4899-1125

Complete contact information is available at: https://pubs.acs.org/10.1021/acsaem.3c02145

Author Contributions

The manuscript was written through contributions of all authors. All authors have given approval to the final version of the manuscript.

Notes

The authors declare no competing financial interest.

ACKNOWLEDGMENTS

Financial support from RSCF (grant no. 19-19-00175) is gratefully acknowledged. Authors thank the Centre for X-ray Diffraction Studies, the Interdisciplinary Resource Centre for Nanotechnology, the Centre for Physical Methods of Surface Investigation, and the Cryogenic Department of the Research Park of St. Petersburg University for performed studies. We also thank Dr. D. A. Lukyanov for the fruitful discussion on our results.

REFERENCES

(1) Steingart, D. Thermophysical Abuse Couplings in Batteries: From Electrodes to Cells. *MRS Bull.* **2021**, *46* (5), 410−419.

(2) Ohsaki, T.; Kishi, T.; Kuboki, T.; Takami, N.; Shimura, N.; Sato, Y.; Sekino, M.; Satoh, A. Overcharge Reaction of Lithium-Ion Batteries. *J. Power Sources* **2005**, *146* (1−2), 97−100.

(3) Chen, Y. Recent Advances of Overcharge Investigation of Lithium-Ion Batteries. *Ionics* **2022**, *28* (2), 495−514.

(4) Lu, L.; Han, X.; Li, J.; Hua, J.; Ouyang, M. A Review on the Key Issues for Lithium-Ion Battery Management in Electric Vehicles. *J. Power Sources* **2013**, *226*, 272−288.

(5) Spotnitz, R. M.; Weaver, J.; Yeduvaka, G.; Doughty, D. H.; Roth, E. P. Simulation of Abuse Tolerance of Lithium-Ion Battery Packs. *J. Power Sources* **2007**, *163* (2), 1080−1086.

(6) Lipu, M. S. H.; Hannan, M. A.; Hussain, A.; Hoque, M. M.; Ker, P. J.; Saad, M. H. M.; Ayob, A. A Review of State of Health and Remaining Useful Life Estimation Methods for Lithium-Ion Battery in Electric Vehicles: Challenges and Recommendations. *J. Clean. Prod.* **2018**, *205*, 115−133.

(7) Zhu, J.; Wierzbicki, T.; Li, W. A Review of Safety-Focused Mechanical Modeling of Commercial Lithium-Ion Batteries. *J. Power Sources* **2018**, *378*, 153−168.

(8) Zhang, S. S.; Xu, K.; Jow, T. R. Enhanced Performance of Li-Ion Cell with LiBF4-PC Based Electrolyte by Addition of Small Amount of LiBOB. *J. Power Sources* **2006**, *156* (2), 629−633.

(9) Wang, F.-M.; Cheng, H.-M.; Wu, H.-C.; Chu, S.-Y.; Cheng, C.-S.; Yang, C.-R. Novel SEI Formation of Maleimide-Based Additives and Its Improvement of Capability and Cyclicability in Lithium Ion Batteries. *Electrochim. Acta* **2009**, *54* (12), 3344−3351.

(10) McMillan, R.; Slegr, H.; Shu, Z. X.; Wang, W. Fluoroethylene Carbonate Electrolyte and Its Use in Lithium Ion Batteries with Graphite Anodes. *J. Power Sources* **1999**, *7*, 20 DOI: 10.1016/S0378-7753(98)00201-8.

(11) Xu, K. Electrolytes and Interphases in Li-Ion Batteries and Beyond. *Chem. Rev.* **2014**, *114* (23), 11503−11618.

(12) Dippel, C.; Schmitz, R.; Müller, R.; Böttcher, T.; Kunze, M.; Lex-Balducci, A.; Röschenthaler, G.-V.; Passerini, S.; Winter, M. Carbene Adduct as Overcharge Protecting Agent in Lithium Ion Batteries. *J. Electrochem. Soc.* **2012**, *159* (10), A1587−A1590.

(13) Lee, H.; Lee, J. H.; Ahn, S.; Kim, H.-J.; Cho, J.-J. Co-Use of Cyclohexyl Benzene and Biphenyl for Overcharge Protection of Lithium-Ion Batteries. *Electrochem. Solid-State Lett.* **2006**, *9* (6), A307.

(14) Ding, J.; Tian, T.; Meng, Q.; Guo, Z.; Li, W.; Zhang, P.; Ciacchi, F. T.; Huang, J.; Yang, W. Smart Multifunctional Fluids for Lithium Ion Batteries: Enhanced Rate Performance and Intrinsic Mechanical Protection. *Sci. Rep.* **2013**, *3* (1), 2485.

(15) Wu, H.; Zhuo, D.; Kong, D.; Cui, Y. Improving Battery Safety by Early Detection of Internal Shorting with a Bifunctional Separator. *Nat. Commun.* **2014**, *5* (1), 5193.

(16) Liu, K.; Liu, Y.; Lin, D.; Pei, A.; Cui, Y. Materials for Lithium-Ion Battery Safety. *Sci. Adv.* **2018**, *4* (6), No. eaas9820.

(17) Xiao, L. F.; Ai, X. P.; Cao, Y. L.; Wang, Y. D.; Yang, H. X. A Composite Polymer Membrane with Reversible Overcharge Protection Mechanism for Lithium Ion Batteries. *Electrochem. Commun.* **2005**, *7* (6), 589−592.

(18) Li, S. L.; Xia, L.; Zhang, H. Y.; Ai, X. P.; Yang, H. X.; Cao, Y. L. A Poly(3-Decyl Thiophene)-Modified Separator with Self-Actuating Overcharge Protection Mechanism for LiFePO4-Based Lithium Ion Battery. *J. Power Sources* **2011**, *196* (16), 7021−7024.

(19) Zhang, L.; Zhang, Z.; Amine, K. Redox Shuttle Additives for Lithium-Ion Battery. In *Lithium Ion Batteries - New Developments*; Belharouak, I., Ed.; InTech, 2012. DOI: 10.5772/26572.

(20) Moshurchak, L. M.; Lamanna, W. M.; Bulinski, M.; Wang, R. L.; Garsuch, R. R.; Jiang, J.; Magnuson, D.; Triemert, M.; Dahn, J. R. High-Potential Redox Shuttle for Use in Lithium-Ion Batteries. *J. Electrochem. Soc.* **2009**, *156* (4), A309.
(21) Moshurchak, L. M.; Buhrmester, C.; Dahn, J. R. Triphenylamines as a Class of Redox Shuttle Molecules for the Overcharge Protection of Lithium-Ion Cells. *J. Electrochem. Soc.* **2008**, *155* (2), A129.
(22) Feng, X. M.; Ai, X. P.; Yang, H. X. A Positive-Temperature-Coefficient Electrode with Thermal Cut-off Mechanism for Use in Rechargeable Lithium Batteries. *Electrochem. Commun.* **2004**, *6* (10), 1021−1024.
(23) Li, H.; Zhang, X.; Zhang, C.; Cao, Y.; Yang, H.; Ai, X.; Zhong, F. Building a Thermal Shutdown Cathode for Li-Ion Batteries Using Temperature-Responsive Poly(3-Dodecylthiophene). *Energy Technol.* **2020**, *8* (7), 2000365.
(24) Beletskii, E. V.; Alekseeva, E. V.; Levin, O. V. Variable-Resistance Materials for Lithium-Ion Batteries. *Russ. Chem. Rev.* **2022**, *91* (3), RCR5030.
(25) Zheng, J.; Wu, X.; Yang, Y. Improved Electrochemical Performance of Li[Li0.2Mn0.54Ni0.13Co0.13]O2 Cathode Material by Fluorine Incorporation. *Electrochim. Acta* **2013**, *105*, 200−208.
(26) Morozov, A. V.; Moiseev, I. A.; Savina, A. A.; Boev, A. O.; Aksyonov, D. A.; Zhang, L.; Morozova, P. A.; Nikitina, V. A.; Pazhetnov, E. M.; Berg, E. J.; Fedotov, S. S.; Tarascon, J.-M.; Antipov, E. V.; Abakumov, A. M. Retardation of Structure Densification by Increasing Covalency in Li-Rich Layered Oxide Positive Electrodes for Li-Ion Batteries. *Chem. Mater.* **2022**, *34* (15), 6779−6791.
(27) Noh, H.-J.; Youn, S.; Yoon, C. S.; Sun, Y.-K. Comparison of the Structural and Electrochemical Properties of Layered Li-[NixCoyMnz]O2 (x = 1/3, 0.5, 0.6, 0.7, 0.8 and 0.85) Cathode Material for Lithium-Ion Batteries. *J. Power Sources* **2013**, *233*, 121−130.
(28) Li, J.; Downie, L. E.; Ma, L.; Qiu, W.; Dahn, J. R. Study of the Failure Mechanisms of $LiNi_{0.8}Mn_{0.1}Co_{0.1}O_2$ Cathode Material for Lithium Ion Batteries. *J. Electrochem. Soc.* **2015**, *162* (7), A1401−A1408.
(29) Kang, Y.; Wang, J.; Du, L.; Liu, Z.; Zou, X.; Tang, X.; Cao, Z.; Wang, C.; Xiong, D.; Shi, Q.; Qian, Y.; Deng, Y. Overcharge Investigations of $LiCoO_2$ /Graphite Lithium Ion Batteries with Different Electrolytes. *ACS Appl. Energy Mater.* **2019**, *2* (12), 8615−8624.
(30) Beletskii, E. V.; Fedorova, A. A.; Lukyanov, D. A.; Kalnin, A. Y.; Ershov, V. A.; Danilov, S. E.; Spiridonova, D. V.; Alekseeva, E. V.; Levin, O. V. Switchable Resistance Conducting-Polymer Layer for Li-Ion Battery Overcharge Protection. *J. Power Sources* **2021**, *490*, No. 229548.
(31) Beletskii, E. V.; Alekseeva, E. V.; Anishchenko, D. V.; Levin, O. V. Li-Ion Battery Short-Circuit Protection by Voltage-Driven Switchable Resistance Polymer Layer. *Batteries* **2022**, *8* (10), 171.
(32) Li, T.; Li, J.; Lu, C.; Wang, L.; Luo, J. Self-Shutdown Function Based on Overcharge-Triggered Electrochemical Nano-Switch for Safer Li-Ion Batteries. *Chem. Eng. J.* **2023**, *452*, No. 139620.
(33) Beletskii, E. V.; Volosatova, Y. A.; Eliseeva, S. N.; Levin, O. V. The Effect of Electrode Potential on the Conductivity of Polymer Complexes of Nickel with Salen Ligands. *Russ. J. Electrochem.* **2019**, *55* (4), 339−345.
(34) Yankin, A. N.; Lukyanov, D. A.; Beletskii, E. V.; Bakulina, O. Yu.; Vlasov, P. S.; Levin, O. V. Aryl-Aryl Coupling of Salicylic Aldehydes through Oxidative CH-activation in Nickel Salen Derivatives. *ChemistrySelect* **2019**, *4* (30), 8886−8890.
(35) Crameri, F. Scientific Colour Maps. *Zenodo* **2018**, DOI: 10.5281/zenodo.2649252.
(36) He, Y.-B.; Ning, F.; Yang, Q.-H.; Song, Q.-S.; Li, B.; Su, F.; Du, H.; Tang, Z.-Y.; Kang, F. Structural and Thermal Stabilities of Layered Li(Ni1/3Co1/3Mn1/3)O2Materials in 18650 High Power Batteries. *J. Power Sources* **2011**, *196* (23), 10322−10327.
(37) Volkov, A. I.; Apraksin, R. V.; Falaleev, E. A.; Novoselova, J. V.; Volosatova, Y. A.; Lukyanov, D. A.; Alekseeva, E. V.; Levin, O. V. Tuning Cationic Transport in Nisalen Polymers via Pseudo-Crown Functionality. *Electrochim. Acta* **2022**, *425*, No. 140750.
(38) Alekseeva, E. V.; Chepurnaya, I. A.; Malev, V. V.; Timonov, A. M.; Levin, O. V. Polymeric Nickel Complexes with Salen-Type Ligands for Modification of Supercapacitor Electrodes: Impedance Studies of Charge Transfer and Storage Properties. *Electrochim. Acta* **2017**, *225*, 378−391.
(39) Lee, M.-H.; Kang, Y.-J.; Myung, S.-T.; Sun, Y.-K. Synthetic Optimization of Li[Ni1/3Co1/3Mn1/3]O2 via Co-Precipitation. *Electrochim. Acta* **2004**, *50* (4), 939−948.
(40) Lepage, D.; Savignac, L.; Saulnier, M.; Gervais, S.; Schougaard, S. B. Modification of Aluminum Current Collectors with a Conductive Polymer for Application in Lithium Batteries. *Electrochem. Commun.* **2019**, *102*, 1−4.
(41) Friel, J. J.; Lyman, C. E. Tutorial Review: X-Ray Mapping in Electron-Beam Instruments. *Microsc. Microanal.* **2006**, *12* (01), 2−25.
(42) Wu, Z.; Ji, S.; Zheng, J.; Hu, Z.; Xiao, S.; Wei, Y.; Zhuo, Z.; Lin, Y.; Yang, W.; Xu, K.; Amine, K.; Pan, F. Prelithiation Activates $Li(Ni_{0.5}Mn_{0.3}Co_{0.2})O_2$ for High Capacity and Excellent Cycling Stability. *Nano Lett.* **2015**, *15* (8), 5590−5596.
(43) Mohanty, D.; Hockaday, E.; Li, J.; Hensley, D. K.; Daniel, C.; Wood, D. L. Effect of Electrode Manufacturing Defects on Electrochemical Performance of Lithium-Ion Batteries: Cognizance of the Battery Failure Sources. *J. Power Sources* **2016**, *312*, 70−79.
(44) Mao, N.; Zhang, T.; Wang, Z.; Cai, Q. A Systematic Investigation of Internal Physical and Chemical Changes of Lithium-Ion Batteries during Overcharge. *J. Power Sources* **2022**, *518*, No. 230767.
(45) Nelson, K. J.; d'Eon, G. L.; Wright, A. T. B.; Ma, L.; Xia, J.; Dahn, J. R. Studies of the Effect of High Voltage on the Impedance and Cycling Performance of $Li[Ni_{0.4}Mn_{0.4}Co_{0.2}]O_2$ /Graphite Lithium-Ion Pouch Cells. *J. Electrochem. Soc.* **2015**, *162* (6), A1046−A1054.
(46) Ma, L.; Xia, J.; Dahn, J. R. Improving the High Voltage Cycling of $Li[Ni_{0.42}Mn_{0.42}Co_{0.16}]O_2$ (NMC442)/Graphite Pouch Cells Using Electrolyte Additives. *J. Electrochem. Soc.* **2014**, *161* (14), A2250−A2254.
(47) Jung, R.; Metzger, M.; Maglia, F.; Stinner, C.; Gasteiger, H. A. Oxygen Release and Its Effect on the Cycling Stability of $LiNi_xMn_yCo_zO_2$ (NMC) Cathode Materials for Li-Ion Batteries. *J. Electrochem. Soc.* **2017**, *164* (7), A1361−A1377.
(48) Spotnitz, R.; Franklin, J. Abuse Behavior of High-Power, Lithium-Ion Cells. *J. Power Sources* **2003**, *113* (1), 81−100.
(49) Kriston, A.; Pfrang, A.; Döring, H.; Fritsch, B.; Ruiz, V.; Adanouj, I.; Kosmidou, T.; Ungeheuer, J.; Boon-Brett, L. External Short Circuit Performance of Graphite-LiNi1/3Co1/3Mn1/3O2 and Graphite-LiNi0.8Co0.15Al0.05O2 Cells at Different External Resistances. *J. Power Sources* **2017**, *361*, 170−181.
(50) Nam, K.-W.; Bak, S.-M.; Hu, E.; Yu, X.; Zhou, Y.; Wang, X.; Wu, L.; Zhu, Y.; Chung, K.-Y.; Yang, X.-Q. Combining In Situ Synchrotron X-Ray Diffraction and Absorption Techniques with Transmission Electron Microscopy to Study the Origin of Thermal Instability in Overcharged Cathode Materials for Lithium-Ion Batteries. *Adv. Funct. Mater.* **2013**, *23* (8), 1047−1063.
(51) Bak, S.-M.; Hu, E.; Zhou, Y.; Yu, X.; Senanayake, S. D.; Cho, S.-J.; Kim, K.-B.; Chung, K. Y.; Yang, X.-Q.; Nam, K.-W. Structural Changes and Thermal Stability of Charged $LiNi_xMn_yCo_zO_2$ Cathode Materials Studied by Combined *In Situ* Time-Resolved XRD and Mass Spectroscopy. *ACS Appl. Mater. Interfaces* **2014**, *6* (24), 22594−22601.
(52) Quilty, C. D.; Bock, D. C.; Yan, S.; Takeuchi, K. J.; Takeuchi, E. S.; Marschilok, A. C. Probing Sources of Capacity Fade in $LiNi_{0.6}Mn_{0.2}Co_{0.2}O_2$ (NMC622): An *Operando* XRD Study of Li/NMC622 Batteries during Extended Cycling. *J. Phys. Chem. C* **2020**, *124* (15), 8119−8128.
(53) Weber, R.; Fell, C. R.; Dahn, J. R.; Hy, S. Operando X-Ray Diffraction Study of Polycrystalline and Single-Crystal $Li_xNi_{0.5}Mn_{0.3}Co_{0.2}O_2$. *J. Electrochem. Soc.* **2017**, *164* (13), A2992−A2999.

https://doi.org/10.1021/acsaem.3c02145
ACS Appl. Energy Mater. XXXX, XXX, XXX−XXX

(54) Li, X.; Xu, M.; Chen, Y.; Lucht, B. L. Surface Study of Electrodes after Long-Term Cycling in Li1.2Ni0.15Mn0.55-Co0.1O2−Graphite Lithium-Ion Cells. *J. Power Sources* **2014**, *248*, 1077−1084.
(55) Madec, L.; Ellis, L. D. Exploring Interactions between Electrodes in Li[Ni $_x$ Mn $_y$ Co $_{1-xy}$]O $_2$ /Graphite Cells through Electrode/Electrolyte Interfaces Analysis. *J. Electrochem. Soc.* **2017**, *164* (14), A3718−A3726.
(56) Guéguen, A.; Streich, D.; He, M.; Mendez, M.; Chesneau, F. F.; Novák, P.; Berg, E. J. Decomposition of LiPF $_6$ in High Energy Lithium-Ion Batteries Studied with Online Electrochemical Mass Spectrometry. *J. Electrochem. Soc.* **2016**, *163* (6), A1095−A1100.
(57) Zhao, W.; Zheng, J.; Zou, L.; Jia, H.; Liu, B.; Wang, H.; Engelhard, M. H.; Wang, C.; Xu, W.; Yang, Y.; Zhang, J. High Voltage Operation of Ni-Rich NMC Cathodes Enabled by Stable Electrode/Electrolyte Interphases. *Adv. Energy Mater.* **2018**, *8* (19), 1800297.
(58) Xu, M.; Li, W.; Lucht, B. L. Effect of Propane Sultone on Elevated Temperature Performance of Anode and Cathode Materials in Lithium-Ion Batteries. *J. Power Sources* **2009**, *193* (2), 804−809.
(59) Lakshminarayanan, P. V.; Toghiani, H.; Pittman, C. U. Nitric Acid Oxidation of Vapor Grown Carbon Nanofibers. *Carbon* **2004**, *42* (12−13), 2433−2442.
(60) Lu, Y.-C.; Mansour, A. N.; Yabuuchi, N.; Shao-Horn, Y. Probing the Origin of Enhanced Stability of "AlPO $_4$ " Nanoparticle Coated LiCoO $_2$ during Cycling to High Voltages: Combined XRD and XPS Studies. *Chem. Mater.* **2009**, *21* (19), 4408−4424.
(61) Bondarchuk, O.; LaGrow, A. P.; Kvasha, A.; Thieu, T.; Ayerbe, E.; Urdampilleta, I. On the X-Ray Photoelectron Spectroscopy Analysis of LiNixMnyCozO2Material and Electrodes. *Appl. Surf. Sci.* **2021**, *535*, No. 147699.
(62) Ahn, W.; Lim, S. N.; Jung, K.-N.; Yeon, S.-H.; Kim, K.-B.; Song, H. S.; Shin, K.-H. Combustion-Synthesized LiNi0.6Mn0.2Co0.2O2 as Cathode Material for Lithium Ion Batteries. *J. Alloys Compd.* **2014**, *609*, 143−149.
(63) Li, D.; Li, H.; Danilov, D. L.; Gao, L.; Chen, X.; Zhang, Z.; Zhou, J.; Eichel, R.-A.; Yang, Y.; Notten, P. H. L. Degradation Mechanisms of C6/LiNi0.5Mn0.3Co0.2O2 Li-Ion Batteries Unraveled by Non-Destructive and Post-Mortem Methods. *J. Power Sources* **2019**, *416*, 163−174.
(64) Haasch, R. T.; Abraham, D. P. Lithium-Based Transition-Metal Oxides for Battery Electrodes Analyzed by x-Ray Photoelectron Spectroscopy. V. LiNi0.4Co0.3Mn0.3O2. *Surf. Sci. Spectra* **2019**, *26* (10), No. 014007.
(65) Gupta, R. P.; Sen, S. K. Calculation of Multiplet Structure of Core p -Vacancy Levels. II. *Phys. Rev. B* **1975**, *12* (1), 15−19.
(66) Grosvenor, A. P.; Biesinger, M. C.; Smart, R. St. C.; McIntyre, N. S. New Interpretations of XPS Spectra of Nickel Metal and Oxides. *Surf. Sci.* **2006**, *600* (9), 1771−1779.

https://doi.org/10.1021/acsaem.3c02145
ACS Appl. Energy Mater. XXXX, XXX, XXX−XXX